Influence of turbulence anisotropy on RANS predictions of wind-turbine wakes

Luan, Yuyang; Dwight, Richard P.

DOI
10.1088/1742-6596/1618/6/062059

Publication date
2020

Document Version
Final published version

Published in
Journal of Physics: Conference Series

Influence of turbulence anisotropy on RANS predictions of wind-turbine wakes

Influence of turbulence anisotropy on RANS predictions of wind-turbine wakes

Yuyang Luan[1], **Richard P. Dwight**[2]

[1,2] Aerodynamics Section, Aerospace Faculty, TU Delft, 2629HT Delft, The Netherlands

E-mail: y.luan@outlook.com, r.p.dwight@tudelft.nl

Abstract. Simulating wind-turbines in Reynolds-averaged Navier-Stokes (RANS) codes is highly challenging, at least partly due to the importance of turbulence anisotropy in the evolution of the wake. We present a preliminary investigation into the role of anisotropy in RANS simulations of vertical-axis turbines, by comparison with LES. Firstly an LES data-set serving as our ground-truth is generated, and verified against previously published works. This data-set provides raw turbulence anisotropy fields for several turbine configurations. This anisotropy is injected into RANS simulations of identical configurations to determine the extent to which it influences (i) the production of turbulence kinetic energy, (ii) the turbulence momentum forcing, and finally (iii) the mean-flow. In all these quantities we observe the anisotropy has a surprisingly limited effect, and is certainly *not* the leading-order error in Boussinesq RANS for these cases. Nevertheless we go on to show that it is feasible to predict anisotropy fields for unseen configurations based only on the mean-flow, by using a tensorized version of random-forest regression.

1. Introduction

In studies of wind farm design, control and maintainance, turbine wake evolution is of great interest for turbine loading as well as power extraction. Several modelling tools have been developed to simulate turbine wakes under the Atmospheric Boundary Layer (ABL). In particular Large Eddy Simulations (LES) has gained popularity as a tool that seems able to reliably predict the majority of the important flow-dynamics, and produce useful predictions for the purposes of scientific study [1, 2]. LES is however much too expensive to be used in an engineering context of real-time control, or farm layout optimization. In these areas, simple empirical models such as Jensen [3] and Larsen [4] models dominate. These are extremely cheap, but include very little physics, relying on sufficient data for fitting, and generally consistent wake behaviour. RANS-based models are in-betweeners, containing lots of physics and therewith the hope of generalizability, but still significantly cheaper than LES. The problem is that the complex nature of the turbulent flow around turbines makes RANS closure models generally quite poor performers in this domain – improving RANS closures for this specific application is therefore a subject of great interest and recent work [5, 6]. For example, one consistent deficit is RANS well-known significant overprediction of turbulence eddy-viscosity in the near-wake, and the consequent much-too-rapid wake recovery [6].

In a similar vein, several authors have noted that turbulence anisotropy in the near-wake is far from Boussinesq – and indeed fitting LES Reynolds-stress tensors to a Boussinesq model implies negative eddy-viscosity in some regions [6]. This observation has been used to explain the failure

of linear eddy-viscosity closures, and the need for (at least) nonlinear eddy-viscosity models (NLEVMs) to acceptably model the flow physics [5]. In spite of this, no currently proposed RANS model for turbines includes a nonlinear eddy-viscosity term – raising the question of whether anisotropy is really critical. Perhaps these anisotropy issues are a subordinate effect, and need only be addressed by the modeller after more important leading-order dominant turbulence modelling effects are correctly treated.

In this work we attempt to quantify the extent to which turbulence anisotropy has a RANS modelling impact. We use LES to generate statistics of mean-flow and Reynolds-stress for a number of multi-turbine configurations, which we use as a ground-truth reference. The normalized turbulence anisotropy b_{ij} of the LES is computed, and injected into a RANS $k-\varepsilon$ model (for the same configuration) in place of the Boussinesq assumption. Thus the reference anisotropy appears in the momentum equation and in production of k and ε, yet no intensity information from the LES is present. We then observe the predicted flow quantities. With some notable exceptions, the presence of the correct anisotropy results in a consistent, but relatively minor improvement in the RANS k-production, turbulence forcing, and mean-flow predictions.

As a final step, we attempt to predict the turbulence anisotropy for unseen flows using a supervised machine-learning framework. This is in the line of previous works on data-driven turbulence modelling by Ling et al. [7], Wu et al. [8], and in mixing-length model fitting for turbines by King et al. [9]. In particular we use the Tensor-Basis Random-Forest (TBRF) method of Kaandorp and Dwight [10]. We train with LES data from one turbine configuration, and predict anisotropy for other configurations, demonstrating the feasibility of this broad approach. We see this work as contributing to the development of effective RANS models for wind-farm simulation.

2. Methodology

We first discuss the generation of our ground-truth LES data for wind-turbines in neutral atmospheric stability conditions using the SOWFA code with actuator-line turbine models, and verify the correctness of these reference results against previous work of Churchfield et al. [11]. Then in Section 2.2 we discuss a steady RANS model of the same problem (with now actuator disc models of the turbines) and note how the Boussinesq assumption results in modelling errors in two terms: the Reynolds-anisotropy tensor, and the turbulence kinetic energy production. These two terms are approximated using the LES data for the same test-case. Finally in Section 3.3 we describe how a random-forest model can be build to describe the anisotropy corrections in terms of the mean-field, in a way that will generalize to other flow cases.

2.1. Large Eddy Simulation of Wind Farms – Reference data generation

We use the wind farm Large Eddy Simulation (LES) solver *SOWFA* [12, 13] which has been developed by the National Renewable Energy Laboratory (NREL). SOWFA is based on the second-order finite-volume solver OpenFOAM, and adds wind-turbine models, boundary-conditions, forcing and turbulence models suitable for the intended application. In particular SOWFA solves the filtered incompressible Navier-Stokes (N-S) equations

$$\frac{\partial \tilde{u}_i}{\partial t} + \frac{\partial \tilde{u}_i \tilde{u}_j}{\partial x_j} = \underbrace{-2\epsilon_{i3k}\Omega_3 \tilde{u}_k}_{\text{Coriolis}} - \frac{1}{\rho_0}\frac{\partial \tilde{p}}{\partial x_i} - \underbrace{\frac{1}{\rho_0}\frac{\partial p_0}{\partial x_i}}_{\text{Driving}} - \frac{\partial \sigma^D_{ij}}{\partial x_j} - \underbrace{\frac{1}{\rho_0} g_3 z \frac{\partial \hat{\rho}}{\partial x_i}}_{\text{Buoyancy}} + \frac{1}{\rho_0} f_i, \tag{1}$$

where $\tilde{\cdot}$ indicates a filtered quantity. Here ρ_0 is the (constant) density, u is velocity, p is pressure without the hydrostatic and driving pressures, and $\partial p_0/\partial x_i$ is a constant horizontal driving pressure-gradient, controlled to establish a target wind-speed at hub-height. The

Cartesian coordinate system is oriented such that x is east, y north and z up, with the ground at $z = 0$, so that Ω_3 is the earth's rotation rate at this latitude of 45°, which is assumed constant across the simulation domain. Turbine forcing is f_i, which is non-zero only near actuator lines. The buoyancy term involving the gravitational force g_3 is modelled by solving the potential temperature transport equation

$$\frac{\partial \tilde{\theta}}{\partial t} + \frac{\partial \tilde{u}_j \tilde{\theta}}{\partial x_j} = \Gamma \frac{\partial^2 \tilde{\theta}}{\partial x_j^2} - \frac{\partial q_j}{\partial x_j}, \tag{2}$$

where the potential temperature θ excludes altitude effects, Γ is the diffusivity and q_j are sub-filter scale temperature fluxes. Given θ, $\hat{\rho}$ is modelled as

$$\frac{\hat{\rho}}{\rho_0} = 1 - \left(\frac{\theta - \theta_0}{\theta_0} \right), \quad \theta_0 = 300\,^\circ\mathrm{K}. \tag{3}$$

The velocity field is subject to the incompressibility constraint $\partial_i \tilde{u}_i = 0$.

SOWFA is generally applied with a precursor simulation of the Atmospheric Boundary Layer (ABL) on a doubly periodic domain, to generate instantaneous inflow conditions for a subsequent simulation with turbine models (as well as identify the driving pressure gradient). In this work the precursor flow domain is $3 \times 3 \times 1$ km and the flow is angled at 240° to avoid grid-alignment effects.

In this work we consider only neutral ABL stability (denoted by 'N') to allow our results to be verified against Churchfield et al. [12, 11]. Two surface roughness heights are simulated: low roughness $z_0 = 0.001$ m (denoted 'L'); and high roughness where $z_0 = 0.2$ m (denoted 'H'). At a reference height of $z_{\mathrm{ref}} = 90$ m (hub height), wind speed is specified to be $\bar{u}_{\mathrm{ref}} = 8$ m/s. Since stability is neutral, an approximately constant $\theta(z) \simeq 300\,^\circ$K profile is expected. Nonetheless to avoid unlimited growth of the ABL, from 700 m to 800 m a capping inversion layer is enforced with a prescribed $\partial\theta/\partial z$ so that $\theta = 308\,^\circ$K at $z = 800$ m. Above this capping inversion layer the potential temperature is approximately constant up to the upper domain boundary. This potential temperature profile is similar to that used by Moeng [14] when simulating neutrally stratified ABLs. Additionally since we are simulating neutral stability, the surface temperature flux $q_{\mathrm{wall},i} = 0$. Finally molecular viscosity $\nu = 1 \times 10^{-5}$ m^2/s while the SGS stresses are modelled by the k-equation eddy-viscosity model [15].

The terrain is flat, and the background mesh is $300 \times 300 \times 100$ structured, yielding a cubic mesh cell size of 10 m. This background mesh is used unmodified in the precursor simulations, but refined near the turbines in the main simulation, yielding 5 m and 2.5 m cell sizes after the first and second refinement levels respectively. Figure 1 illustrates the refinement, as well as the three turbine configurations considered in this study. In Figure 1(a) the baseline case is shown with only one turbine; (b) shows two parallel turbines at $3D$ apart; and (c) two sequential turbines $7D$. All turbines in Figure 1 are approximated by the actuator line model proposed by Sørensen and Shen [16] with the Gaussian width set to twice the cell size around the turbines.

2.2. Reynolds-averaged Navier-Stokes with injected anisotropy

While reasonably accurate, LES is too computationally expensive to be practical for applications such as wind-farm layout optimization or control. Therefore we consider steady Reynolds-averaged Navier-Stokes (RANS) as an alterative. However many authors have observed that standard RANS models perform poorly when predicting wind-turbine wakes - for example the eddy viscosity in the wake is consistently over-estimated, leading to a much too rapid wake recovery. In particular, Rethore [6] identified a large region immediately behind the turbine where Boussinesq (in $k - \varepsilon$) gives non-realizable predictions for the Reynolds-stress tensor, and regions where the eddy-viscosity computed from LES is negative. We therefore

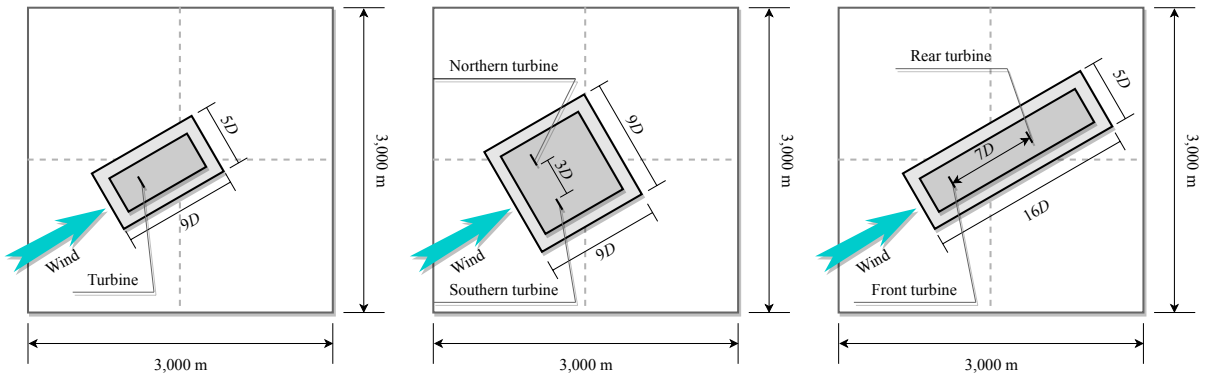

(a) OneTurbine (b) ParallelTurbines (c) SequentialTurbines

Figure 1: Wind farm layout top view for three configurations involving one or two turbines. Grey regions indicate 5 m and 2.5 m refined mesh-cells respectively.

identify Boussinesq closures as fundamentally inadequate model for these flows, and examine the magnitude of the resulting error, as well as the possibility of correcting it.

The exact Reynolds-averaged governing equations for the wind-farm are:

$$\frac{\partial \langle u_i \rangle}{\partial t} + \frac{\partial \langle u_i \rangle \langle u_j \rangle}{\partial x_j} = -2\epsilon_{i3k}\Omega_3 \langle u_k \rangle - \frac{1}{\rho_0}\frac{\partial \langle p \rangle}{\partial x_i} - \frac{1}{\rho_0}\frac{\partial p_0}{\partial x_i} + \frac{\partial \nu \langle S_{ij} \rangle}{\partial x_j} - \frac{\partial \tau_{ij}}{\partial x_j} - \frac{1}{\rho_0} g_3 z \frac{\partial \langle \hat{\rho} \rangle}{\partial x_i} + \frac{1}{\rho_0}\hat{f}_i, \quad (4)$$

and $\partial_i \langle u_i \rangle = 0$, where $\langle \cdot \rangle$ is the Reynolds averaging operator. The terms correspond one-to-one with those of (1), with the exception that $\hat{f}_i$ now represents forcing due to actuator disc(s), and the nonlinear convection term results in a Reynolds stress tensor $\tau_{ij} := \langle u_i' u_j' \rangle$, where $u_i' := u_i - \langle u_i \rangle$ is the fluctuating part of the velocity. The tensor τ_{ij} can be written in isotropic and anisotropic parts $\tau_{ij} = a_{ij} + \frac{2}{3}k\delta_{ij}$ where the turbulence kinetic energy $k := \frac{1}{2}\tau_{ii}$, and the normalized anisotropy $b_{ij} := a_{ij}/2k$.

The closure problem for RANS consists of providing a model for τ_{ij} in terms of averaged quantities only. In the incompressible case the isotropic part of τ_{ij} has no effect of the mean velocity, being directly countered by pressure. We therefore only need model a_{ij}. A Boussinesq closure is one that employs the model

$$a_{ij} \simeq a_{ij}^B := -\nu_T S_{ij}, \quad (5)$$

where ν_T is some *turbulence viscosity*, which is typically identified via transport models for k and some turbulence time-scale – e.g. in the $k-\varepsilon$ model. In these equations τ_{ij} also appears, notably in the production term in the exact k-equation $P_k = \tau_{ij}\partial_j u_i$, where it is also replaced with a Boussinesq approximation.

In the following we solve the RANS equations with (A) the unmodified $k-\varepsilon$ model of [17] (i.e. Boussinesq), and (B) a model with b_{ij} injected from the corresponding LES simulation. In this second solve $b_{ij} = b_{ij}^{\text{LES}}$ is fixed, and used wherever it appears in the equations (in the momentum equation, and production terms in k and ε equations). As such only the anisotropy information from the LES is used, and no information about mean-flow or turbulence intensity. By comparing the results of (A), (B) and the LES, we can directly observe the impact of the Boussinesq assumption on the mean-flow, and the extent to which the RANS model is corrected by introducing a "correct" turbulence anisotropy.

While this procedure is useful to identify turbulence anisotropy modelling error, it is not useful for prediction. For that it is necessary to predict b_{ij} based on resolved quantities.

2.3. Supervised machine-learning predictions of normalized turbulence anisotropy

In order to make predictions we therefore need to approximate b_{ij}^{LES} as a function of $\langle u \rangle$, k, and other quantities resolved by the RANS simulation, i.e. a tensor-valued regression problem. Given such a function f we directly have a turbulence closure based on the LES data, and we might hope that it: (1) reproduces the LES training case mean-flow when applied within a RANS solver, and (2) generalizes to similar cases. In the case of wind-farms, we ultimately aim to train f from LES simulations of multiple pairs of turbines, and apply it to entire farms – although this ambition is far from realized in this paper.

Before solving the regression problem, we identify a few reasonable properties for f. Like turbulence itself, f should be (i) Galilean invariant, (ii) invariant under rotations. These constraints dictate use of the well-known finite base-tensor series of Pope [18]:

$$b_{ij}^{\mathrm{LES}} \simeq f(S_{ij}, \Omega_{ij}, c) = \sum_{m=1}^{10} T_{ij}^{(m)}(S_{ij}, \Omega_{ij}) g^{(m)}(\lambda_1, \lambda_2, ..., \lambda_5, c) \tag{6}$$

where $T_{ij}^{(m)}$ are the tensor bases, $T_{ij}^{(1)} := S_{ij}$, $T_{ij}^{(2)} := S_{ik}\Omega_{kj} - \Omega_{ik}S_{kj}$, etc. [10], λ_m are the corresponding scalar invariants, and c are additional Galilean invariant scalar features. It remains to identify the arbitrary scalar functions $g^{(m)}(\cdot)$ to regress the data.

At this point we follow the work of Kaandorp and Dwight [10], who developed the Tensor-Basis Random-Forest (TB-RF) inspired by previous works in neural-networks by Ling et al. [19, 7], and random-forests by Wu et al. [8]. Random-forests consist of averages of multiple decision trees. Decision trees approximate data by recursively splitting the input-space into bins along Cartesian directions, and approximating the function as constant within each bin. Which variable to split, and the location of the split are chosen by a greedy procedure, minimizing the data misfit at each step. The TB-RF generalizes this to approximate tensors of the the form (6). In particular at each split we solve:

$$\min_{j,s} \left(\min_{g_L^{(m)} \in \mathbb{R}^{10}} \sum_{n \in R_L(j,s)} \left\| \sum_{m=1}^{10} \mathbf{T}_n^{(m)} g_L^{(m)} - \mathbf{b}_n^{\mathrm{LES}} \right\|_F^2 + \min_{g_R^{(m)} \in \mathbb{R}^{10}} \sum_{n \in R_R(j,s)} \left\| \sum_{m=1}^{10} \mathbf{T}_n^{(m)} g_R^{(m)} - \mathbf{b}_n^{\mathrm{LES}} \right\|_F^2 \right), \tag{7}$$

where j is the index of the input variable to split, s is the location of the split, and n indexes the LES data-points (one at each cell of the LES mesh). Also $R_L(j,s)$, $R_R(j,s)$ are the sets of data points in the bins on the left and right of the split respectively, and $g_L^{(m)}$, $g_R^{(m)}$, are the values of the function in the left and right bins. The norm is the Frobenius norm.

The TB-RF was used successfully in [10] for predicting two-dimensional flows in channels and square-ducts, and showed the ability to generalize within that limited set of flows. The flows considered here are substantially less varied from a flow-physics standpoint, and therefore we expect similar performance. As a result of its speed it can be readily extended to large numbers of input features, and we use the set of 50 features used by Wu et al. [8].

3. Results

First we verify our LES reference simulations against previous work; secondly we show the effect of directly injecting LES anisotropy b_{ij}^{LES} into RANS simulations of the same flow case; finally we demonstrate the ability of the TB-RF regression model to predict b_{ij} for an unseen flow.

3.1. LES ground-truth verification

Figure 2 presents the time-averaged inflow velocity, turbulence intensity profiles as well as the instantaneous energy spectrum at hub height z_{hub} of our LES precursor for neutral stability, and

low-roughness conditions. The results are substantially similar to reported data from Churchfield et al. [11]. Differences are visible in the velocity profile near the inversion layer, likely due to differing numerical treatment of the layer. Our grid is slightly coarser, leading to a somewhat reduced energy in the spectrum. Note that Figure 2(b) includes SGS variance, while Figure 2(c) does not, accounting for the difference in the integrated spectra.

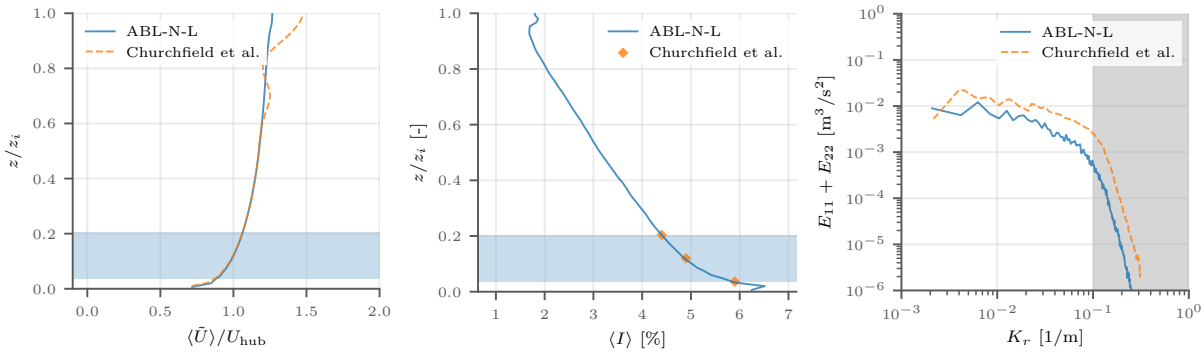

(a) Mean velocity profile (b) Mean turbulence intensity profile (c) Energy spectrum at z_{hub}

Figure 2: Validation of the ABL-N-L LES precursor with Churchfield et al. [11].

Figure 3 shows the 0.0275 s^{-2} isosurface Q-criterion, for the instantaneous field of the N-L-SequentialTurbines case after 23 000 s of physical time. Only the second refinement region as depicted in Figure 1 has been visualized. In the front turbine wake, vortex breakdown and wake expansion can be clearly identified. Moreover, bound and tip vortices are clearly visible. The rear turbine has a more rapid wake expansion as expected, and only small vortical structures are visible.

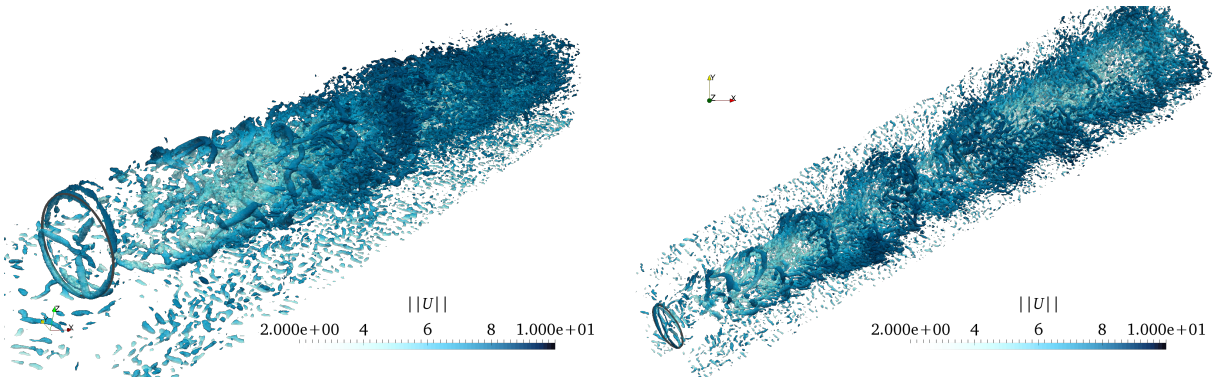

Figure 3: Two perspectives of the isosurface of Q-criterion for N-L-SequentialTurbines after 23,000 s of simulation time. The isosurface is coloured by the time-averaged velocity magnitude.

Finally, the normalized hub height horizontal velocity deficit magnitude $|\Delta\langle\tilde{u}\rangle_{\text{hor}}|$ profile is presented in Figure 4 and is compared to [11]. The wake profile of this simulation closely resembles that from Churchfield both in magnitude as well as shape. We consider the correctness of the reference data hereby verified, and continue with use of the data.

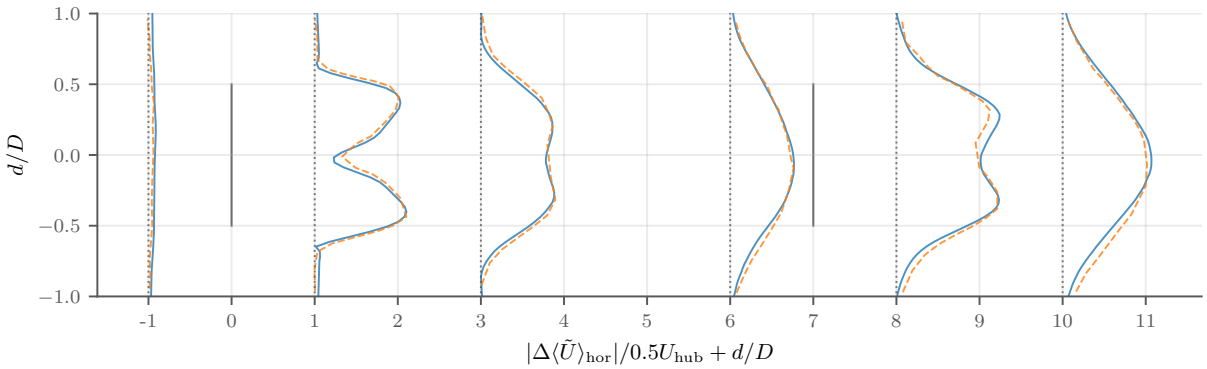

Figure 4: Normalized $|\Delta\langle\tilde{u}\rangle_{\mathrm{hor}}|$ profile for N-L-SequentialTurbines LES (——) and Churchfield et al. [11] (- - - -) at z_{hub}, sampled -1D, +1D, +3D w.r.t. the front and rear turbines.

3.2. Reynolds-averaged Navier-Stokes with injected LES anisotropy

We now inject the LES normalized turbulence anisotropy b_{ij}^{LES} into the RANS equations, following Section 2.2, whereby important to remember is that predictions of k and the mean-velocity originate in RANS, only b_{ij} is artificially supplied. The resulting prediction of production of turbulence kinetic energy P_k is shown in Figure 5, comparing baseline $k-\varepsilon$, $k-\varepsilon$ with $k-\varepsilon$ injection, and the LES reference for two turbine configurations. In both configurations, injection produces minor improvements of the magnitude and shape of P_k, except close to the disc (1D profiles) where minor degradation is observed most likely due to the direct effect of the rotor forcing on the turbulence, which is not accounted for in either RANS model. Note that P_k depends on b_{ij} via $P_k = 2k(b_{ij} + \frac{1}{3}\delta_{ij})\partial_j u_i$, i.e. the alignment of b_{ij} with the velocity-gradient tensor influences production [20]. However the magnitude of P_k is still controlled to a large extent by k. In this figure therefore the shape is enhanced by injection – most notably near the hub region, where baseline RANS misses the production peaks completely, while small peaks are visible in injected RANS. Of course the magnitude is still clearly under-predicted everywhere, highlighting that this anisotropy-corrected production term, does not lead to a sufficiently increased k in the shear layers. We can deduce that anisotropy alone is responsible for only a very small part of the k deficit we observe here, and other modelling effects are needed to account for the majority.

Similar considerations apply to the prediction of turbulence forcing in the momentum equation caused by the $\partial_j\tau_{ij}$ term. Once more b_{ij} controls primarily the spatial extent, and k the magnitude of the forcing, so we would expect the former to be significantly improved, and the latter less so. This expectation is borne out in Figure 6, which plots the magnitude of the horizontal component of this forcing $(\partial_j\tau_{ij})_{\mathrm{hor}}$. In addition we can observe a gradual improvement of $(\partial_j\tau_{ij})_{\mathrm{hor}}$ downstream, hinting that the dominant modelling error is made close to the turbine (perhaps at the actuator model itself), and that anisotropy may be of increasing importance in the medium- and far-wake.

Finally, when it comes to mean velocity field, the improvement due to more accurate b_{ij} is most prominent for the vertical velocity component, $\langle\mathbf{u}_z\rangle$, but even there the effect is relatively minor. By inspecting the wake profiles in Figure 7, we observe a consistent oscillation pattern on the northern side of the turbine in the reference data (due to the tip vortices) that is completely missing from the baseline RANS. Hints of the same structure begin to appear downstream in the injected RANS, but once again, the effect of turbulence anisotropy is swamped by larger modelling errors.

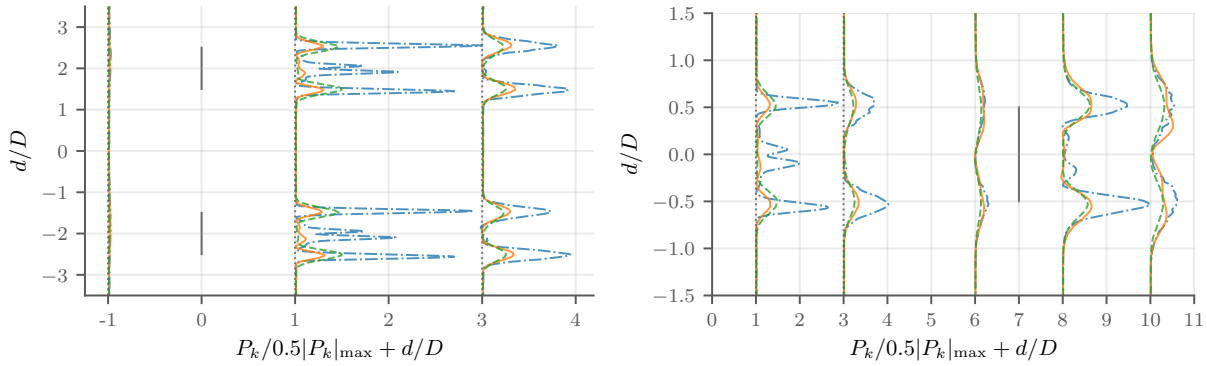

(a) N-L-ParallelTurbines (b) N-L-SequentialTurbines

Figure 5: Normalized hub height P_k for N-L-ParallelTurbines and N-L-SequentialTurbines at z_{hub} from LES (— · —), RANS with b_{ij}^{LES} injection (——), and baseline RANS (- - - -), sampled at -1D, +1D, and +3D w.r.t. turbine locations.

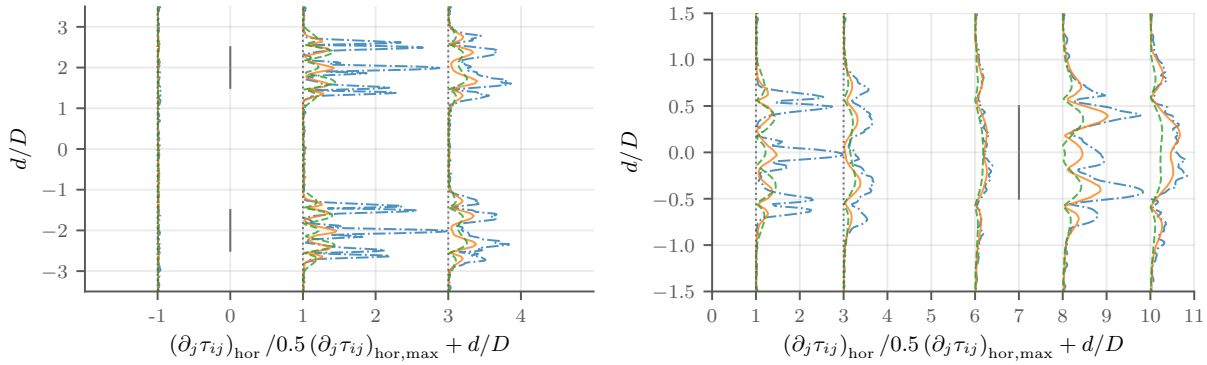

(a) N-L-ParallelTurbines (b) N-L-SequentialTurbines

Figure 6: Normalized $(\partial_j \tau_{ij})_{\text{hor}}$ profile for N-L-ParallelTurbines and N-L-SequentialTurbines at z_{hub} using LES (— · —), RANS with b_{ij}^{LES} injection (——), and baseline RANS (- - - -).

3.3. Machine Learning Predictions of the Turbulence Anisotropy Tensor

In Figure 8, barycentric color-maps of the N-H-ParallelTurbines case at z_{hub}, z_{mid}, and z_{apex} are presented. The color-maps capture the anisotropy character, in terms of its position within the barycentric triangle (a transformed version of the Lumley triangle) [21]. Blue represents three-component turbulence, green two-component and red one-component, etc. The baseline RANS result is the Boussinesq prediction, and bears no relation to the reference. The reference still contains streaks in the boundary-layer, indicating that the LES is not sufficiently averaged to eliminate these relatively long-lived structures. The TBRF prediction reproduces the character of the LES very well, including the streaks, but also introduces a lot of noise into the prediction, especially upstream of the turbine. This is a familiar feature of random-forest predictions, which are unaware of spatial relationships, including correlation. To be used as a turbulence model, significant smoothing would be required.

Finally, the normalized profiles of P_k for N-L-SequentialTurbines are shown in Figure 9 for both TBRF and a competing method: Tensor-Basis Adaptive Boosting (TBAB). As the turbine configuration is sequential, horizontal lines at hub height and -1D, +1D, +3D w.r.t. the front

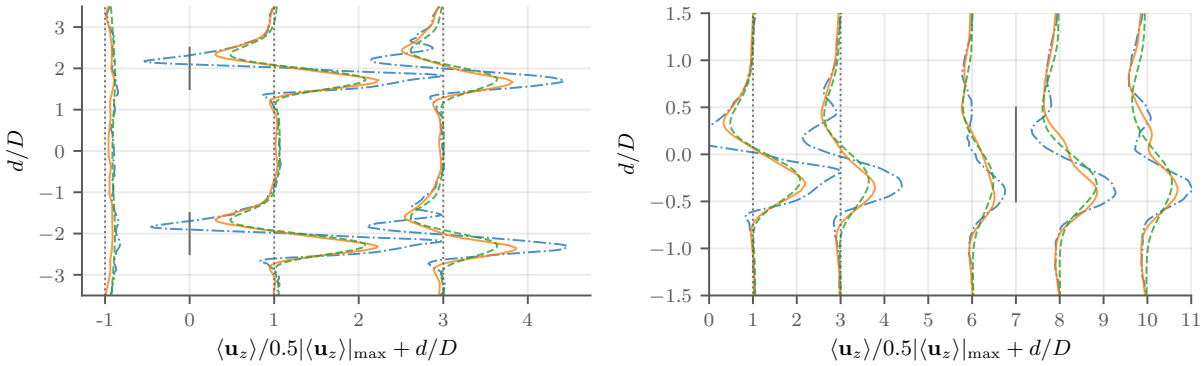

(a) N-L-ParallelTurbines (b) N-L-SequentialTurbines

Figure 7: Normalized $\langle \mathbf{u}_z \rangle$ profile for N-L-ParallelTurbines and N-L-SequentialTurbines at z_{hub} using LES (— · —), RANS with b_{ij}^{LES} injection (——), and baseline RANS (- - - -).

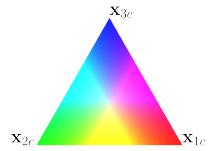

(a) Barycentric map

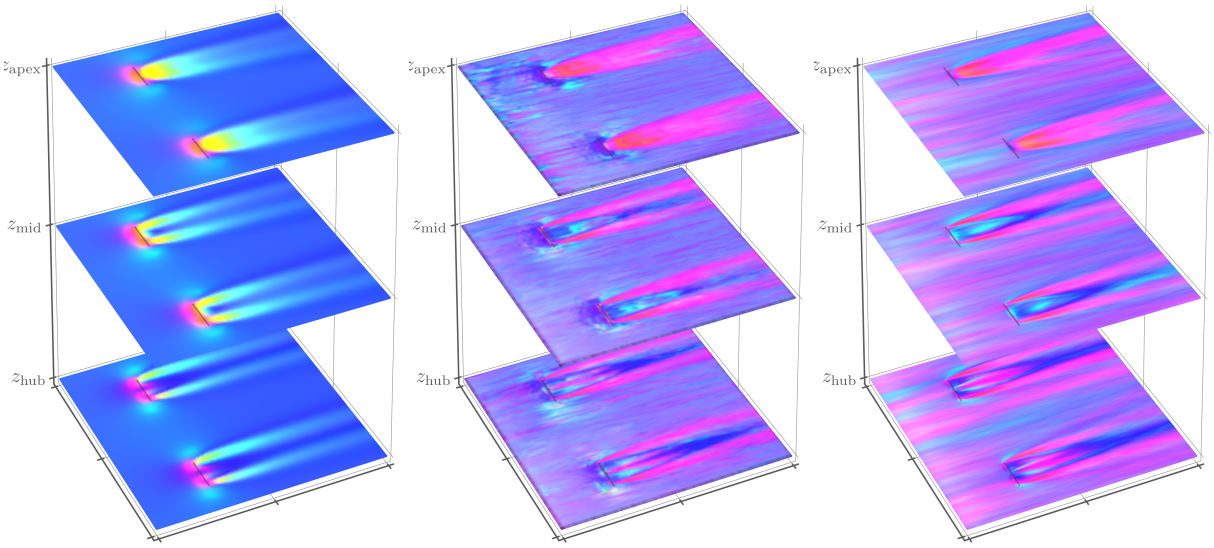

(b) RANS (c) TBRF prediction (d) LES

Figure 8: Barycentric map at z_{hub}, z_{mid}, and z_{apex} for N-H-ParallelTurbines using RANS, TBRF prediction after training on the N-H-OneTurbine LES ground truth, and LES

and rear turbines are plotted. The higher turbulent intensity upstream of the rear turbine is visible. Opposite to the front turbine where the northern side of its tip free shear layer has a larger P_k, the rear turbine has a higher P_k at the southern side of the tip free shear layer. All these effects are reproduced by both regression methods.

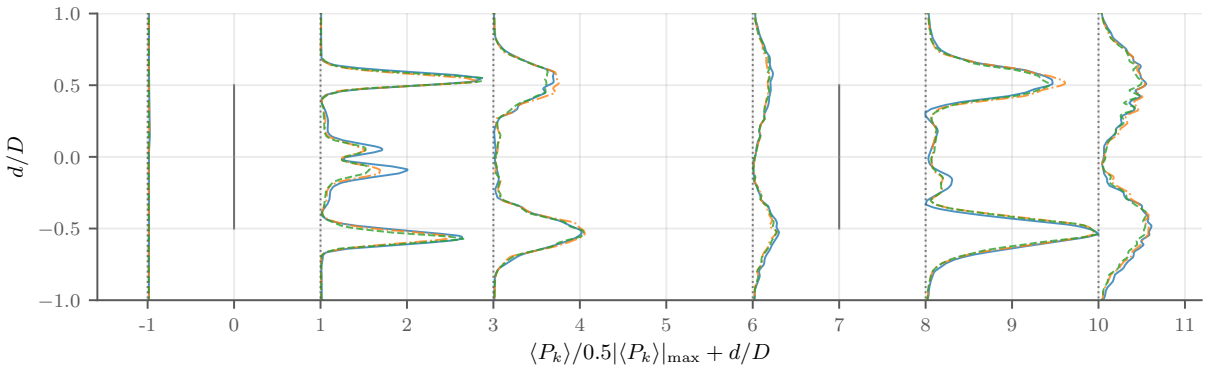

Figure 9: P_k profile of N-L-SequentialTurbines at z_{hub} from LES (——), TBRF (— · —), and TBAB (- - - -) prediction, sampled at $-1D$, $+1D$, and $+3D$.

4. Conclusions & Recommendations

We have quantified the effect of turbulence anisotropy in isolation on the accuracy of RANS models for wind-turbines. The corrective effect of using the LES anisotropy are much smaller than might be supposed, and suggest modelling efforts should first focus on correcting other, dominating effects. Notable are the under-predictions of k in the strong shear layer, and near-wake effects due to the actuator model. Our results suggest anisotropy might play a more important role in the mid- to far-wake. Reproducing turbulence anisotropy with random-forest-like models works reasonably well in the configurations we considered. Further work must consider the effect of ABL stability on wake development – this is challenging from both a data-generation and a model generalization point-of-view.

Acknowledgments

Bart Matthijs Doekemeijer and Julia Steiner provided valuable support throughout this work.

References

[1] Stevens R J and Meneveau C 2017 *Annual Review of Fluid Mechanics* **49** 311–339
[2] Calaf M, Meneveau C and Meyers J 2010 *Physics of Fluids* **22** 015110
[3] Jensen N O 1983 *A note on wind generator interaction* (Risø National Laboratory)
[4] Frandsen S 2007 *Turbulence-generated structural loading in wind turbine clusters* Ph.D. thesis DTU
[5] van der Laan P 2014 *Efficient Turbulence Modeling for CFD Wake Simulations* (DTU Wind Energy)
[6] Réthoré P 2009 *Wind Turbine Wakes in Atmospheric Turbulence* Ph.D. thesis DTU
[7] Ling J, Kurzawski A and Templeton J 2016 *Journal of Fluid Mechanics* **807** 155–166 ISSN 0022-1120
[8] Wu J L, Xiao H and Paterson E 2018 *Phys. Rev. Fluids 3, 074602 (2018)*
[9] King R N, Adcock C, Annoni J and Dykes K 2018 *Journal of Physics: Conference Series* **1037** 072004
[10] Kaandorp M L A and Dwight R P 2020 *Computers and Fluids (to appear), arXiv:1810.08794*
[11] Churchfield M J, Lee S, Michalakes J and Moriarty P J 2012 *Journal of Turbulence* **13** N14
[12] Churchfield M, Lee S, Moriarty P, Martinez L, Leonardi S, Vijayakumar G and Brasseur J 2012 *AIAA 2012-0537 (doi:10.2514/6.2012-537)*
[13] Martínez-Tossas L A, Churchfield M J and Leonardi S 2014 *Wind Energy* **18** 1047–1060
[14] Moeng C H and Sullivan P P 1994 *Journal of Atmospheric Sciences* **51** 999–1022
[15] Deardorff J W 1980 *Boundary-Layer Meteorology* **18** 495–527 ISSN 1573-1472
[16] Sørensen J N and Shen W Z 2002 *Journal of Fluids Engineering* **124** 393–399 ISSN 0098-2202
[17] Hossain M and Rodi W 1982 *Turbulent Buoyant Jets and Plumes* pp 121 – 178 ISBN 978-0-08-026492-9
[18] Pope S B 1975 *Journal of Fluid Mechanics* **72** 331–340 ISSN 0022-1120
[19] Ling J, Jones R and Templeton J 2016 *Journal of Computational Physics* **318** 22–35 ISSN 0021-9991
[20] Pope S B 2012 *Turbulent Flows* (Cambridge University Press) ISBN 9780511840531
[21] Emory M and Iaccarino G 2014 *Center for Turbulence Research Annual Research Briefs*